THE JOURNAL OF BIOLOGICAL CHEMISTRY VOL. 286, NO. 7, pp. 5736–5743, February 18, 2011

Structural Characterization of the Complex between α-Naphthoflavone and Human Cytochrome P450 1B1*

Received for publication, November 17, 2010 Published, JBC Papers in Press, December 8, 2010, DOI 10.1074/jbc.M110.204420

An Wang[‡], **Uzen Savas**[‡], **C. David Stout**[§1], **and Eric F. Johnson**[‡2]

From the Departments of [‡]*Molecular and Experimental Medicine and* [§]*Molecular Biology, The Scripps Research Institute, La Jolla, California 92037*

The atomic structure of human P450 1B1 was determined by x-ray crystallography to 2.7 Å resolution with α-naphthoflavone (ANF) bound in the active site cavity. Although the amino acid sequences of human P450s 1B1 and 1A2 have diverged significantly, both enzymes exhibit narrow active site cavities, which underlie similarities in their substrate profiles. Helix I residues adopt a relatively flat conformation in both enzymes, and a characteristic distortion of helix F places Phe[231] in 1B1 and Phe[226] in 1A2 in similar positions for π-π stacking with ANF. ANF binds in a distinctly different orientation in P450 1B1 from that observed for 1A2. This reflects, in part, divergent conformations of the helix B′-C loop that are stabilized by different hydrogen-bonding interactions in the two enzymes. Additionally, differences between the two enzymes for other amino acids that line the edges of the cavity contribute to distinct orientations of ANF in the two active sites. Thus, the narrow cavity is conserved in both P450 subfamily 1A and P450 subfamily 1B with sequence divergence around the edges of the cavity that modify substrate and inhibitor binding. The conservation of these P450 1B1 active site amino acid residues across vertebrate species suggests that these structural features are conserved.

Enzymes of the cytochrome P450 (CYP) superfamily play a significant physiologic role in the detoxication of foreign compounds and the biosynthesis of endogenous compounds, including steroid hormones, bile acids, and cholesterol. P450 [3] families 1, 2, 3, and 4 contribute most extensively to the transformation of xenobiotics to more polar metabolites that can be better excreted. In humans and most mammals, family 1 comprises three well studied enzymes: P450s 1A1, 1A2, and 1B1. P450 1A2 is expressed mainly in liver, whereas P450s 1B1 and 1A1 are expressed in many extrahepatic organs. Transcription of the corresponding genes is activated by aryl hydrocarbon receptor (AhR), a transcription factor that binds planar aromatic hydrocarbons, and P450s 1A and 1B oxidize a variety of polycyclic aromatic hydrocarbons (1). Some of their metabolites are carcinogenic, and P450 1B1 is uniquely associated with the carcinogenicity of dimethylbenzanthracene in a mouse model of tumorigenesis (2).

Additionally, P450 family 1 enzymes contribute to metabolism of endogenous compounds that include 17β-estradiol, retinals, arachidonic acid, and melatonin. In contrast to P450 1A enzymes, 1B1 is highly conserved throughout vertebrate evolution, suggesting an important physiologic function. Consistent with this notion, allelic variants of the *CYP1B1* gene are associated with an increased risk for glaucoma (3, 4), but the underlying mechanism is unclear. Expression of the *CYP1B1* gene is also regulated conditionally by the estrogen receptor (ER) and cAMP-response element-binding protein (CREB) (5, 6). Elevated expression of P450 1B1 has been reported for a number of tumors of breast, prostate, ovary, lung, and brain origin, and it has been suggested that selective inhibition would potentially prevent formation of active carcinogens and inactivation of anti-cancer agents (7). Alternatively, pro-drug activation by 1B1 in cancer cells could be feasible for treatment of malignancies (8).

In this study, we determined the structure of human P450 1B1 by x-ray diffraction to better understand the structural basis for functional similarities and differences exhibited by family 1 P450s. Human P450 1B1 shares only 38 and 36% amino acid sequence identity with human P450s 1A1 and 1A2, respectively, but shares an overlapping profile of substrates with the family 1A enzymes. The enzyme was crystallized with α-naphthoflavone (ANF)[4] bound in the active site cavity. ANF is a potent inhibitor of P450 family 1 enzymes, with an IC_{50} of 4, 6, and 60 nM for human P450s 1B1, 1A2, and 1A1, respectively (9). Although the amino acid sequence conservation is relatively low, our results indicate that P450 1B1 exhibits a narrow, slot-like substrate binding cavity similar to the one characterized previously for human P450 1A2 (10). This planar and compact active site of family 1 P450s is distinct from the active site architectures exhibited by other xenobiotic metabolizing enzymes in P450 families 3A and 2. Although this feature is shared by P450s 1B1 and 1A2, the orientation of the bound ANF differs between the two en-

* This work was supported, in whole or in part, by National Institutes of Health Grant GM031001 (to E. F. J.).

The atomic coordinates and structure factors (code 3pm0) have been deposited in the Protein Data Bank, Research Collaboratory for Structural Bioinformatics, Rutgers University, New Brunswick, NJ (http://www.rcsb.org/).

[1] To whom correspondence may be addressed: Dept. of Molecular Biology, The Scripps Research Institute, 10550 N. Torrey Pines Rd., MB8, La Jolla, CA 92037. Tel.: 858-784-8738; Fax: 858-784-2857; E-mail: dave@scripps.edu.

[2] To whom correspondence may be addressed: Dept. of Molecular and Experimental Medicine, The Scripps Research Institute, 10550 N. Torrey Pines Rd., MEM-255, La Jolla, CA 92037. Tel.: 858-784-7918; Fax: 858-784-7978; E-mail: johnson@scripps.edu.

[3] P450 is a generic term for a cytochrome P450 enzyme; individual P450s are identified using a number-letter-number format based on amino acid sequence relatedness.

[4] The abbreviations used are: ANF, α-naphthoflavone; r.m.s., root mean square.

zymes and reflects the extensive amino acid sequence divergence between the two enzymes. These structural differences between the two enzymes are likely to underlie differences in catalytic properties for the two enzymes.

EXPERIMENTAL PROCEDURES

Expression and Purification of Human P450 1B1—Expression vectors were designed to produce modified forms of human P450 1B1 in *Escherichia coli* using an approach previously described for expression and crystallization of human microsomal P450 1A2 (10). The N-terminal amino acid sequence was truncated by replacing codons for the first 50 residues with a nucleotide sequence encoding the shorter amino acid sequence, MAKKTSSKGK. This approach has been used for expression and crystallization of other microsomal P450s (11). The substitute sequence replaced all amino acid residues upstream of the proline-rich motif at the beginning of the catalytic domain and removed the N-terminal transmembrane domain to increase solubility and to eliminate a flexible appendage. Additionally, the coding sequence was extended by adding codons for 4 histidine residues at the C terminus to enable affinity purification of the modified P450 using nickel-nitrilotriacetic acid-agarose (Qiagen, Chatsworth, CA) affinity chromatography. The P450 1B1 expression vector was generated from a cDNA that corresponds to the functional *CYP1B1*2* allele bearing two missense mutations: R48G (reference SNP: rs10012) and A119S (reference SNP: rs1056827). Residue 48 occurs in the linker region and was replaced by the N-terminal substitution in the expression vector. The A119S mutation occurs on the solvent-exposed surface of the helix B-C loop. The modified coding region was inserted into the pCWori plasmid.

E. coli strain DH5α was co-transformed with the P450 1B1 expression plasmid and the pGro7 plasmid for elevated expression of the chaperones GroEL and GroES (Takara Bio Inc., Shiga, Japan). Cells harboring both plasmids were selected based on their ability to grow on LB plates containing ampicillin and chloramphenicol. Protein expression and purification conditions were adopted and optimized based on protocols for the expression and purification of P450 1A2 (10). A single ampicillin- and chloramphenicol-resistant colony was used to inoculate 10 ml of LB medium containing both antibiotics and cultured at 37 °C and 220 rpm overnight. The cell suspension was transferred into 500 ml of terrific broth supplemented with ampicillin and chloramphenicol and incubated at 37 °C with shaking at 220 rpm in a tabletop C24KC refrigerated incubator/shaker (New Brunswick Scientific, Edison, NJ) until an optical density of 0.5 at 660 nm was reached. Then, the temperature was lowered to 30 °C with shaking at 190 rpm. When the optical density at 660 nm reached 0.7–0.8, δ-aminolevulinic acid (5 mM), isopropyl-β-D-thiogalactopyranoside (1 mM), and arabinose (4 g/liter) (Sigma-Aldrich) were added to induce the expression of P450 1B1 and of GroES and GroEL, respectively. After 24 h, cells were harvested, and crude lysates were prepared as described previously (10). Protein was kept in a buffer containing 20 mM potassium phosphate (potassium P_i, pH 7.4), 300 mM NaCl, 20% glycerol, 20 μM ANF, 10 mM β-mercaptoethanol, and 10 mM CHAPS detergent (Anatrace, Maumee, OH) with 1 mM phenylmethylsulfonyl fluoride during cell lysis and protein extraction. P450 1B1 was purified by a nickel-nitrilotriacetic acid-agarose (Qiagen, Valencia, CA) affinity column and size-exclusion chromatography using Sephacryl S-200 (Sigma-Aldrich). Following centrifugal concentration, the protein was used for crystallization. The concentration of the protein was estimated by UV-visible difference spectroscopy for the CO-complex of the dithionite-reduced enzyme *versus* the reduced enzyme. The protein is a monomer in solution based on size-exclusion chromatography using an FPLC system with a Superdex 200 HR 10/30 column (Amersham Biosciences).

Protein Crystallization—The modified P450 1B1 protein was crystallized by hanging drop vapor diffusion. Drops containing 1.25 μl of nominally 400 μM P450 1B1, 0.625 μl of protein buffer, and 0.625 μl of precipitant solution (20% PEG-3350, 0.2 M ammonium dibasic citrate, pH 5.1) were set to equilibrate against 0.5 ml of reservoir solution composed of the same precipitant solution with 500 mM NaCl at 296 K. Protein crystals formed after 1 week as clusters of single plates. To grow single crystals, microseeding was used. A crystal cluster was ground to produce microcrystals and suspended in 150 μl of a 1:3 solution of precipitant solution and protein buffer using a glass tissue grinder. The suspension was serially diluted 1:4, and in most cases, the third or fourth serial dilution worked well for crystal growth. The hanging drop was composed of 0.25 μl of the diluted suspension of microcrystals, 1 μl of protein solution (nominally 350 μM), 0.625 μl of protein buffer, and 0.625 μl of the precipitant solution.

Structure Determination—A dataset to 2.7 Å resolution, collected at the Stanford Synchrotron Radiation Laboratory beam line 7-1 for a single crystal (size 0.2 × 0.1 × 0.02 mm) belonging to space group $P2_12_12$ was used to build and refine the final model. Data collection and model refinement statistics are summarized in Table 1. The crystal was flash-frozen in liquid nitrogen, and the diffraction data were collected at 100 K. The CCP4 programs MOSFLM and SCALA (12) were used to process the data. Initial phasing was obtained by molecular replacement using Phaser (13) employing a pruned P450 1B1 homology model. The homology model was generated by Modeler (14) using the structure of P450 1A2 (Protein Data Bank (PDB): 2hi4) as the template. External loops and portions of the N terminus were deleted to reduce clashes in the lattice packing detected during the molecular replacement search. Model building and comparison with electron density maps using COOT were iterated with refinement of the atomic coordinates and individual *B*-factors by simulated annealing and/or minimization using CNS (15).

RESULTS AND DISCUSSION

Our objective was to determine the atomic structure of human P450 1B1 to provide fundamental information for understanding the structure and function of the enzyme. Additionally, a better understanding of the structural similarities and differences exhibited by P450 1B1 relative to the P450 1A family was sought. P450 1B1 exhibits an amino acid identity of <40% with respect to human family 1A enzymes, which would typically lead to designation as a separate P450 family.

Nevertheless, P450 1B1 exhibits similar functional and regulatory characteristics when compared with family 1A enzymes, which led to its designation as subfamily 1B.

P450 1B1 was expressed in a modified form for crystallization. Microsomal P450s are targeted to the endoplasmic reticulum by a leader sequence that is retained as the only transmembrane component of the enzyme. The leader sequence and linker were replaced by a short sequence related to the linker sequence of P450 2C3 (16–18) that has served well for expression and crystallization of other microsomal P450s. The protein was crystallized in the presence of ANF, a high affinity reversible inhibitor of the enzyme that binds in the substrate binding cavity. Additionally, ANF was present throughout the isolation procedure to stabilize the protein. The protein crystallized in the space group $P2_12_12$, and the protein model was built and refined using x-ray diffraction data scaled and integrated to 2.7 Å. A molecular replacement solution for a single molecule of P450 1B1 in the asymmetric unit was obtained using a homology model constructed from the published structure of P450 1A2 (PDB: 2hi4) (10). This required removal of several external loops as well as the N-terminal residues preceding helix A from the model because of clashes in the crystal lattice. Additionally, several regions were poorly predicted by the homology model and required extensive rebuilding and fitting during the construction of the final P450 1B1 model.

Overall, the P450 1B1 polypeptide chain is longer than that of P450 1A2 (Fig. 1). The C terminus of P450 1B1 extends for 17 amino acids beyond the C terminus of P450 1A2. Only the 6 most proximal residues of the extended C terminus were defined well by electron density and could be modeled. These residues of the 1B1 protein extended away from the canonical fold of the catalytic domain and packed against other molecules in the crystal lattice. Additionally, the N terminus preceding helix A and the loop between helix H and I could not be modeled completely.

TABLE 1
Data collection and refinement statistics

P450 construct		1B1dH
Data collection		
No. of crystals		1
Complex		α-naphthoflavone (ANF)
Space group		$P2_12_12$
Unit cell		
a, *b*, *c* (Å)		84.17, 103.98, 62.97
α, β, γ		90°, 90°, 90°
SSRL beam line		BL 7–1
Wavelength (Å)		0.98
Resolution range (Å) (outer shell)		65.5–2.7 (2.85–2.7)
Total observations		115,381
Unique reflections > 0.0 σ_F		15,741
Completeness %[a]		99.6 (100)
$\langle I/\sigma_I \rangle$[a]		5.7 (1.7)
R_{symm} (I)[a]		0.110 (0.438)
Refinement		
R-factor		0.235
R_{free} (5% of data)		0.278
r.m.s. deviation bonds (Å)		0.0099
r.m.s. deviation angles (degrees)[b]		1.49
Residues/No. of atoms/average *B*-factor (Å²)		
Protein[c]	3656	46.03
Heme	43	29.06
ANF	21	40.48
Water	33	35.50

[a] Values for the highest resolution shell in parentheses.
[b] Ramachandran plot: 86.4% of residues in most favored regions; 12.8% in allowed regions; 0.2% in generously allowed regions; 0.5% in disfavored regions.
[c] Residues 68–307 and 312–530 of modified P450 1B1. There was insufficient density to model residues 51–67, 308–311, and 531–547. Therefore, they were not included in the final model.

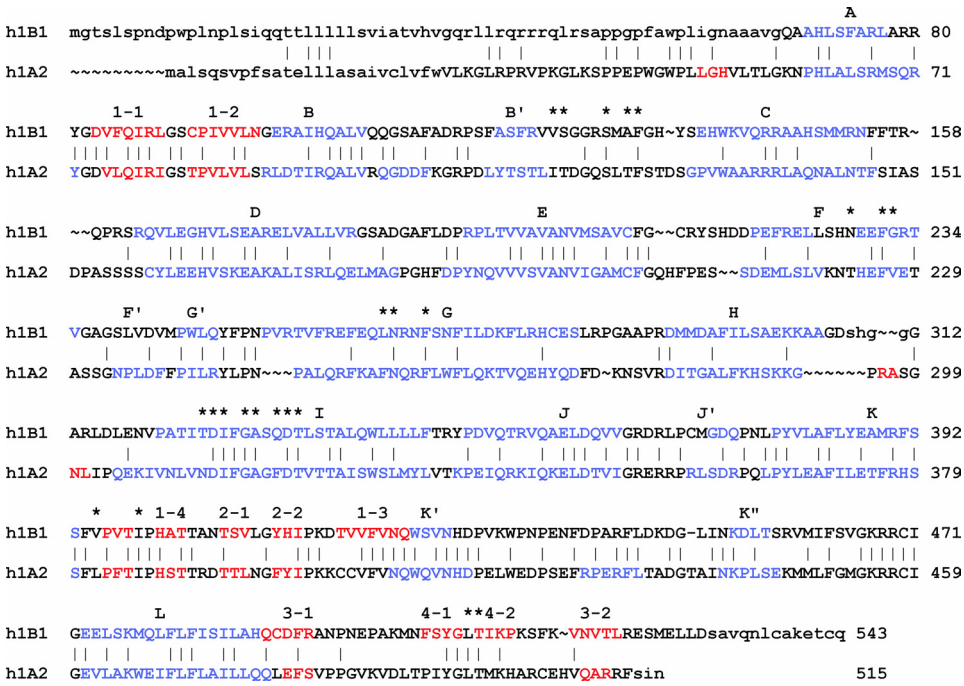

FIGURE 1. **Structure-based amino acid sequence alignment of human (*h*) P450s 1B1.2 and 1A2.1.** Helical and extended secondary structures are shown in *blue* and *red type*, respectively, and are labeled alphabetically for helices and numerically for sheets and strands above the sequence of h1B1. Residues that were not modeled in the structure are shown in *lowercase*. The *asterisks* denote residues that reside in the active site cavities of the two enzymes (Table 2). The *vertical bars* denote amino acid identity. Native N-terminal sequences are shown, but each was truncated for expression in *E. coli* and subsequent crystallization.

As seen in Fig. 1, differences are evident in the lengths of α-helices and β-sheets as well as for external loops between elements of secondary structure. Although the two structures could be superimposed with an overall 1.33 Å r.m.s. deviation for structurally aligned Cα carbons, the external loops between the helices C and D, D and E, F and G, G and H, and H and I, strand β3-1 and β4-1, and adjacent residues exhibited significantly larger r.m.s. deviations of 3 Å to >10 Å. The r.m.s. deviation for β-sheet 1 and helix F was also significantly greater than the mean. Additionally, the α-helical hydrogen-bonding pattern is lost for both proteins at ^{226}SHN^{228} for P450 1B1 and ^{221}KNT^{223} for P450 1A2, causing one helical turn in the middle of helix F to unwind as it crosses above the substrate binding cavity. Thus, this unusual feature is maintained in the structures of both proteins. This distortion contributes to features of the substrate binding cavity.

TABLE 2

Active site amino acid residues of human P450s 1B1 and 1A2 as well as corresponding residues in 1A1

Active site amino acid residues conserved between P450s 1B1 and 1A2, and assumed for 1A1, are shown in bold typeface. Residues with no active site exposure are italicized. Corresponding residues for human P450 1A1 are shown. Almost all of the 1B1 active site amino acids are conserved across vertebrate species as is Lys^{512}, which forms a salt bridge with Asp^{333}. Exceptions are noted (*). h, human.

h-1B1	h-1A1	h-1A2
B-C loop		
Val^{126}	Ile^{115}	Ile^{117}
Ser^{127}	Ser^{116}	Thr^{118}
Ser^{131}*	**Ser^{120}**	**Ser^{122}**
Ala^{133}	Ser^{122}	Thr^{124}
Phe^{134}	**Phe^{123}**	**Phe^{125}**
F helix		
Asn^{228}	Asn^{221}	Thr^{223}
Phe^{231}	**Phe^{224}**	**Phe^{226}**
*Gly^{232}**	Gly^{225}	Val^{227}
G helix		
Leu^{264}	Leu^{254}	Phe^{256}
Asn^{265}	**Asn^{255}**	**Asn^{257}**
Phe^{268}	**Phe^{258}**	**Phe^{260}**
I helix		
Thr^{325}*	Leu^{312}	Asn^{312}
Asp^{326}	**Asp^{313}**	**Asp^{313}**
Gly^{329}	**Gly^{316}**	**Gly^{316}**
Ala^{330}	**Ala^{317}**	**Ala^{317}**
Gln^{332}	Phe^{319}	Phe^{319}
Asp^{333}	**Asp^{320}**	**Asp^{320}**
Thr^{334}	**Thr^{321}**	**Thr^{321}**
Helix K to β1 Loop		
Val^{395}*	Val^{382}	Leu^{382}
Ile^{399}	**Ile^{386}**	**Ile^{386}**
β4 Turn		
Leu^{509}	**Leu^{496}**	**Leu^{497}**
Thr-510	**Thr^{497}**	**Thr^{498}**
Lys$_{512}$	**Lys^{499}**	***Lys$_{500}$***

Although the overall sequence identity is low between human P450s 1B1 and 1A2 (<38%), the conservation of amino acid residues residing in the active site cavity is higher with 13 of 22 being conserved (Table 2). A similar degree of conservation is evident for a sequence alignment with human P450 1A1. The conservation of the amino acid residues in the active site cavity of P450 1B1 across vertebrate sequences is even higher, 18 of 20. The total number of residues in P450 1B1 is smaller because of structural differences that obscure 2 residues seen in the active site of 1A2 from exposure in the active site cavity of 1B1. This high degree of conservation is generally not seen for xenobiotic metabolizing P450s in family 2, where the gain and loss of genes through gene duplication and divergence during evolution has led to extensive structural and functional diversity for their active site cavities. In contrast, a single *CYP1B1* gene is generally seen in vertebrate genomes (19, 20).

The orientation and position of ANF in the active site cavity are defined by a $2|F_o| - |F_c|$ σA-weighted electron density map calculated for a model that did not include ANF (Fig. 2). The orientation of the ANF molecule shown in Fig. 2 on the *left* is the best match for the electron density as indicated by the envelope of the electron density map. The phenyl ring is close to the heme iron with two closest carbon atoms at <5 Å from the heme iron, which places them close to the reactive heme iron-oxo intermediate formed during catalysis. An alternative orientation, shown on the *right* in Fig. 2, can largely be accommodated within the electron density, but the alternative ANF model does not account for all of the observed density between the phenyl ring and the benzo(h)chromen-4-one moiety leading to significant peak in the $|F_o| - |F_c|$ elec-

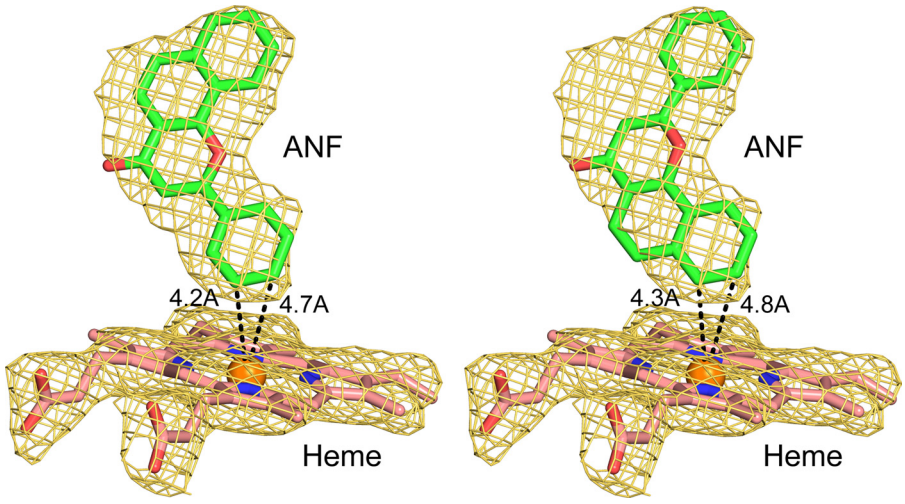

FIGURE 2. **An unbiased $2|F_o| - |F_c|$ σA-weighted electron density ANF omit map (*gold mesh*) is shown contoured at 1σ around the heme and ANF molecules depicted as *stick figures*.** ANF was modeled as shown on the *left* with a less likely alternative orientation shown on the *right*.

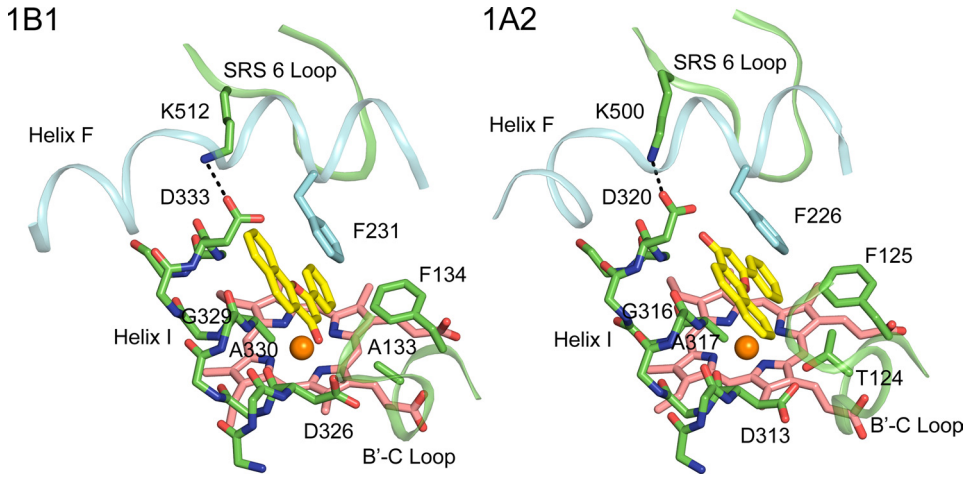

FIGURE 3. **ANF binds in a narrow activity site cavity of P450 1B1 that is similar to that of P450 1A2.** Helix I forms one wall of the slot. Helix F distorts as it crosses the slot and places a conserved Phe (Phe^{231} and Phe^{226}) so that the aromatic side chain stacks against ANF. A second conserved Phe (Phe^{134} and Phe^{125}) on the BC loop also borders the slot. ANF and heme are rendered with *yellow* and *pink carbons*, respectively. Note the different orientations of ANF in the two active site cavities.

tron density map contoured at 3σ. Evaluation of the two orientations using XSCORE (21) indicated highly similar interaction energies for the two orientations, and it is possible that the latter binding orientation might also occur to a lesser extent than the first orientation. Although ANF is a potent competitive inhibitor of family 1 P450s, ANF is reported to be oxidized to more polar, unidentified products by P450 1B1 *in vitro* (9). The products of ANF oxygenation by human P450 1A1 expressed in yeast have been identified as the 5,6-epoxide (22), whereas rat P450 1A1 is reported to produce both the 7,8-epoxide and the 5,6-epoxide (23). These metabolites would be more consistent with the alternative positioning of the ANF shown in Fig. 2, *right panel*, which positions the 7 and 8 carbons closest to the heme iron.

ANF binds in a narrow slot-like active site cavity above the surface of the heme. One side of the slot is defined by helix I (Fig. 3). The flat surface of ANF rests against the relatively flat surface formed by the peptide bond between Gly^{329} and Ala^{330} of helix I, where the methyl group of Ala^{330} is almost aligned in the plane of the peptide bond. Two phenylalanine residues, 134 and 231, form the opposite side of the slot. These amino acid residues are highly conserved in human P450s 1B1, 1A1, and 1A2 (Table 2). In the three-dimensional structures of both 1B1 and 1A2, helix F bends and distorts as it crosses over the slot and the salt bridge formed by Asp and Lys residues that are conserved in both proteins. The distortion positions a conserved Phe for interaction with the ANF although the residues forming helix F are not conserved generally between the two proteins. This distortion of helix F is not typically seen in other P450s and alters the direction of the helix F axis.

Despite the similarity of the active site architectures, ANF binds in distinctly different orientations in P450s 1B1 and 1A2. This reflects differences in the shapes of the active site cavities (Fig. 4) that reflect, in turn, differences of amino acid residues that form the edges of the cavities (Table 2) as well as differences in polypeptide backbone conformation. The solvent-accessible surfaces of the cavities were calculated using

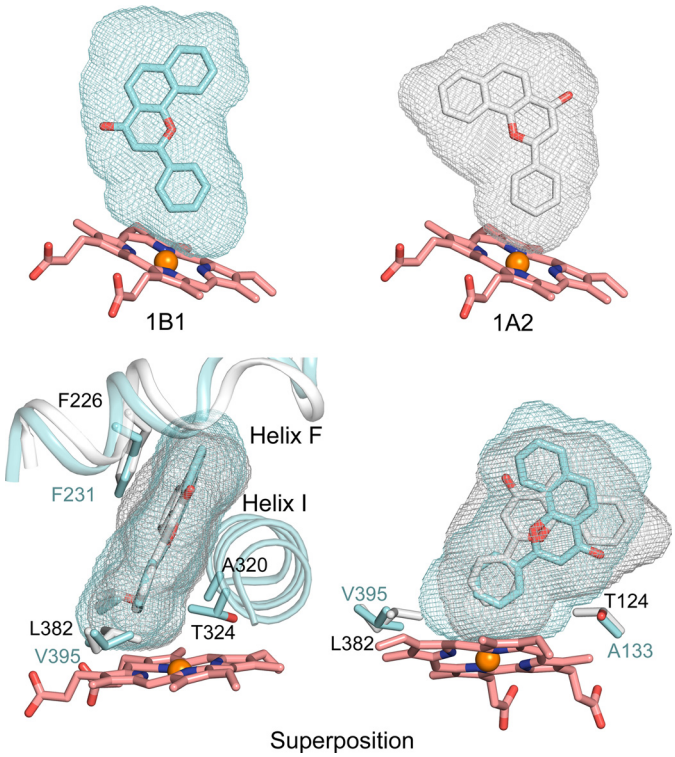

FIGURE 4. **Solvent-accessible surfaces of the substrate binding cavities of P450s 1B1 and 1A2 are rendered as *mesh surfaces*.** Side views are shown for each enzyme (*top*), and a superposition of the two is shown as an edge view and an opposing side view (helix I removed) (*bottom*). Carbons are colored *cyan*, *gray*, and *pink* for 1B1, 1A2, and the heme, respectively.

VOIDOO (24) and are depicted in Fig. 4 as *mesh surfaces* to illustrate the overall size and shape of each cavity. The overall size of the P450 1B1 cavity is 398 Å^3, which is very similar to the 375 Å^3 volume of the 1A2 cavity (10). In contrast, much larger differences are evident between P450s in family 2 where cavities range in size from 190 Å^3 for P450 2E1 (25) to 1438 Å^3 for P450 2C8 (26).

From the edge view of the superimposed active site cavities of P450s 1B1 and 1A2 in Fig. 4, the planarity of the active site

is well conserved between P450s 1B1 and 1A2. However, from the side view of the superimposed active site cavities of P450s 1B1 and 1A2, different shapes are readily apparent. Two critical residues corresponding to Val^{395} and Ala^{133} of P450 1B1 contribute to differences in the cavity shapes near the surface of the heme (Fig. 4, Table 2). Val^{395} in P450 1B1 could give extra space for substrate binding when compared with Leu^{382} in P450 1A2. Interestingly, Val^{395} of P450 1B1 is conserved as Val^{382} in P450 1A1. This critical residue has been studied by Szklarz and co-workers (27) through mutation, and the reciprocal P450 1A1 V382L and P450 1A2 L382V mutants display interchanged preferences for 7-ethoxyresorufin *O*-deethylation *versus* 7-methoxyresorufin *O*-demethylation reflecting the extra space provided by the valine side chain for the ethoxy group.

Both active site cavities are closed without solvent or substrate access channels when ANF is bound, implying that the structure must open to allow access and egress of ligands to and from the active site cavity. This is most likely to occur at the intersections of the helix I, the helix G, and the helix B-C loop as predicted by the program Mole (28), and this prediction is consistent with observations that this region is flexible in other P450s such as P450 2C5 (11, 29). The displacements involve changes arising from torsion angle motion of the B-C loop and changes in the pitch of helix G that can be accompanied by deflection of the pitch of the N-terminal end of helix I at the intersection of these three elements of secondary structure.

The high affinity observed for the binding of ANF to both enzymes is likely to reflect, in large part, the binding of the planar aromatic compound between the hydrophobic walls that form the narrow cavity. The enzymes may not exhibit a similarly closed and compact shape when structurally dissimilar substrates bind such as the pro-carcinogen dibenzo(a,l)pyrene diol, which is activated to a very potent mutagen and carcinogen by 1B1 (30). This is also likely to occur for the binding of 17β-estradiol to both enzymes due to the out-of-plane methyl group and reduced planarity of the unsaturated rings of estradiol. Interestingly, the two enzymes exhibit different regiospecificities for the oxygenation of the phenolic ring of 17β-estradiol. 4-Hydroxylation predominates for 1B1, whereas 2-hydroxylation is favored for 1A2 and 1A1 (31). This is likely to reflect differences in the steric constraints of the two active site cavities.

Differences in the shapes of the two cavities where helix G, I, and the B-C loop meet arise from different conformations of the B-C loop as well as differences for amino acid residues on the B-C loop and helix I, as illustrated in Fig. 5. Although a reduction in the size of the side chains of Val^{126}, Ser^{127}, Ala^{133}, and Thr^{325} relative to the corresponding residues in P450 1A2, Ile^{117}, Thr^{118}, Thr^{124}, and Asn^{312}, has the potential to increase the volume of the 1B1 active site cavity, these changes are offset to some extent by differences in the conformation of the helix B-C loop, which closes in on the bound ANF in the distal portion of the cavity. Differences in the hydrogen-bonding networks involving the conserved aspartic acid, Asp^{326} and Asp^{313} for 1B1 and 1A2, respectively, contribute to divergent conformations of the B-C loop. In 1A2, hydrogen bonding is evident between Thr^{124} and Asp^{313}, whereas the side chain of the corresponding Ala^{133} cannot hydrogen-bond to the Asp^{326}. Asp^{326} forms a hydrogen bond with the amide hydrogen of Ala^{313} as well as the hydroxyl side-chains of Ser^{127} and Ser^{131}. These interactions stabilize a conformation of the B-C loop that differs from that of 1A2. As illustrated in Fig. 5, *B* and *C*, by the *dashed line*, the carbonyl oxygen of the ANF molecule could form a hydrogen bond with the Asp^{326}. As the protein was crystallized in an acidic environment (~pH 5.0), the hydrogen bonding between the carbonyl and Asp^{326} may be favored, whereas protonation of Asp^{326} is less likely at neutral pH even in this buried environment. The ANF molecule is constrained by steric interactions in the cavity so that the position of the carbonyl is juxtaposed with Asp^{326}. In contrast, two water molecules are found in the 1A2 cavity that form a hydrogen-bonded chain between Asp^{313} of 1A2 and Thr^{118} in a more open conformation of the helix B-C loop. Interestingly, human P450 1A1 is likely to be more closely related to the structure of P450 1A2 because Ser^{122}, which corresponds to Thr^{124} of 1A2, would support a similar hydrogen-bonding pattern.

Fig. 5*B* displays portions of each structure that form the opposite, upper corners of the substrate binding site cavities of the two enzymes. This corner is formed by helix F as it crosses the cavity and over the conserved salt bridge between Asp^{333} on helix I and Lys^{512} on β-sheet 4. This salt bridge is conserved in 1A2 between Asp^{320} and Lys^{500}, and these residues are conserved in P450 1A1 as well (Table 2). In P450 1A2, Asp^{320} forms hydrogen bonds with Thr^{510} on β-sheet 4 and with Thr^{223} on helix F as well. These hydrogen bonds are not evident for the structure of P450 1B1-ANF complex due to a substitution of Asn^{228} for the corresponding Thr^{223} and the displacement of β-sheet 4, which distances the corresponding Thr^{510} from Asp^{333}. This appears to reflect, in part, the hydrogen bonding of Asn^{228} on helix F of P450 1B1, which corresponds to Thr^{223} of 1A2, with Gln^{332} on helix I. This is likely to contribute to differences in the threading of helix F over the active site and β-sheet 4. A void is also created that accommodates a water molecule near Gly^{232}. The side chain of Val^{227} in P450 1A2 occupies the space utilized by the water in P450 1B1. On the other hand, the side chains of the P450 1B1 hydrogen-bonded pair, Asn^{223} and Gln^{332}, occupy space utilized by a water molecule in 1A2, which forms a hydrogen bond with the carbonyl of ANF and with a carbonyl in the backbone of helix I. The interaction of the Asn^{228} and Gln^{332} significantly reduces the active site space and shifts the position of Phe^{268} on helix G relative to the corresponding residue, Phe^{260}, in P450 1A2. Additionally, the side chain of P450 1B1 Leu^{264} occupies somewhat less space than the corresponding Phe^{256} of 1A2. Collectively, these differences contribute significantly to the distinct shapes of the active site cavities of the two enzymes. As summarized in Table 2, 8 of 20 amino acid residues found in the active site cavity of P450 1B1 differ from the corresponding residues in P450 1A2, and all but 2 of the 20 residues are highly conserved in P450 1B1 across vertebrate species from teleosts to primates. Moreover, differences in the backbone conforma-

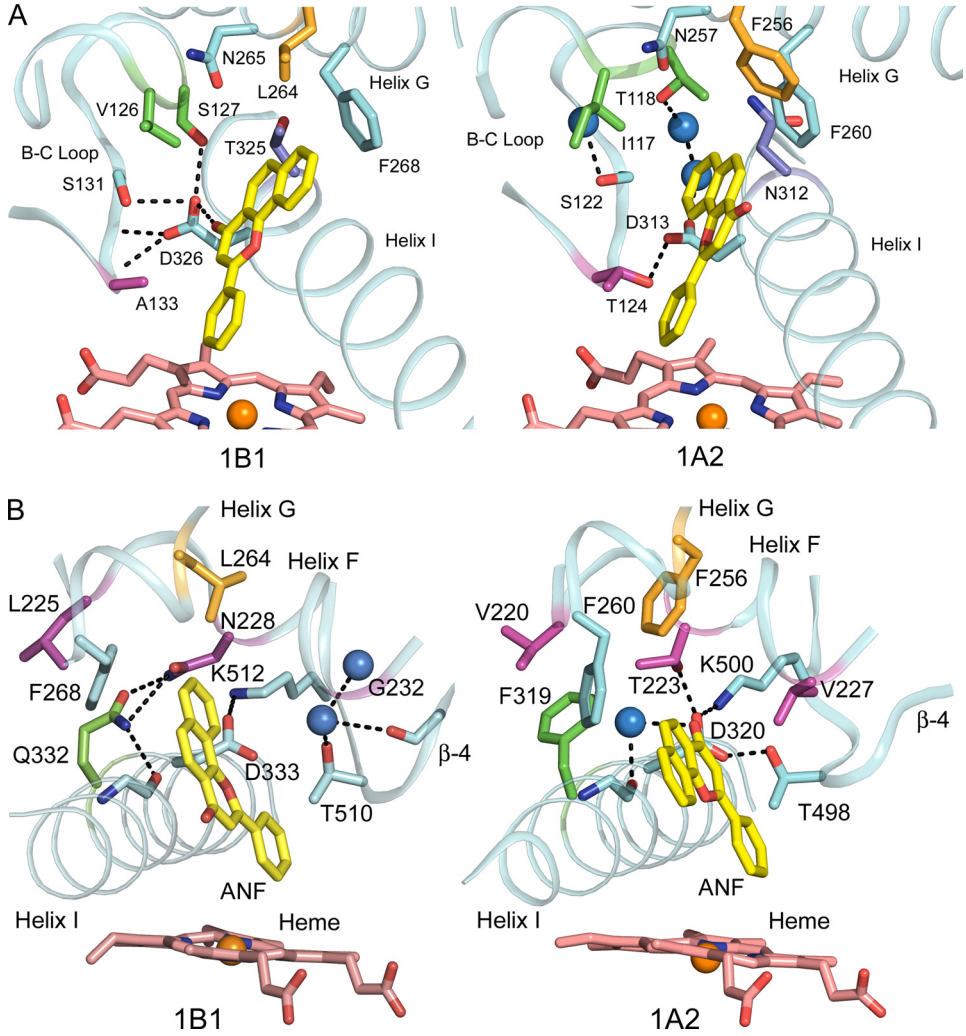

FIGURE 5. **Structural features forming the upper corners of substrate binding cavity.** *A* and *B* correspond to the left and right corners of the cavity as viewed in Fig. 4 (*top*). Conserved amino acids are shown with *cyan* carbons, whereas differing residues have carbons rendered with alternative colors. Water molecules are shown as *blue spheres*. Hydrogen bonding is depicted by *dashed lines*.

tion of P450 1A2 increase the volume of the cavity near the helix B-C loop and expose 2 additional residues in the cavity.

In summary, the structure of human P450 1B1 demonstrates similarities and differences when compared with the structure of P450 1A2. A conservation of the overall topology of the active site cavity indicates selective pressure to maintain a slot-like active site that is well adapted for binding hydrophobic, planar polynuclear aromatic ring systems such as those exhibited by flavonoids and polynuclear aromatic hydrocarbons. Hydrophobic interactions with the sides of the slot are likely to be the predominant interaction that contributes to binding affinity. The distal edges of the slot exhibit a mix of hydrophobic and polar residues. The latter contribute both to the stability of the slot through highly conserved residues, hydrogen bonding, and electrostatic interactions as well as to differences in cavity shape that arise from sequence differences. In this regard, the hydrogen bond donors typically found in family 1A P450s that correspond to P450 1B1 Ala^{133} contribute significantly to differences in the conformation of the B-C loop observed for human P450s 1B1 and 1A2. The binding site residues of P450 1B1 are highly conserved across vertebrate species, suggesting a strong functional selection that is likely to reflect a role in metabolism of endogenous substrates that may underlie the contributions of the *CYP1B1* genetic variation to congenital glaucoma (3, 4).

Acknowledgments—Portions of the research were carried out at the Stanford Synchrotron Radiation Lightsource (SSRL), a national user facility operated by Stanford University on behalf of the United States Department of Energy, Office of Basic Energy Sciences. The SSRL Structural Molecular Biology Program is supported by the United States Department of Energy, Office of Biological and Environmental Research, and by the National Center for Research Resources, Biomedical Technology Program, and NIGMS of the National Institutes of Health.

REFERENCES

1. Nebert, D. W., Dalton, T. P., Okey, A. B., and Gonzalez, F. J. (2004) *J. Biol. Chem.* **279,** 23847–23850
2. Buters, J. T., Sakai, S., Richter, T., Pineau, T., Alexander, D. L., Savas, U., Doehmer, J., Ward, J. M., Jefcoate, C. R., and Gonzalez, F. J. (1999) *Proc. Natl. Acad. Sci. U.S.A.* **96,** 1977–1982

3. Vasiliou, V., and Gonzalez, F. J. (2008) *Annu. Rev. Pharmacol. Toxicol.* **48,** 333–358
4. Choudhary, D., Jansson, I., and Schenkman, J. B. (2009) *Xenobiotica* **39,** 606–615
5. Zheng, W., Brake, P. B., Bhattacharyya, K. K., Zhang, L., Zhao, D., and Jefcoate, C. R. (2003) *Arch. Biochem. Biophys.* **416,** 53–67
6. Sissung, T. M., Price, D. K., Sparreboom, A., and Figg, W. D. (2006) *Mol. Cancer Res.* **4,** 135–150
7. Chun, Y. J., and Kim, S. (2003) *Med. Res. Rev.* **23,** 657–668
8. Bruno, R. D., and Njar, V. C. (2007) *Bioorg. Med. Chem.* **15,** 5047–5060
9. Shimada, T., Yamazaki, H., Foroozesh, M., Hopkins, N. E., Alworth, W. L., and Guengerich, F. P. (1998) *Chem. Res. Toxicol.* **11,** 1048–1056
10. Sansen, S., Yano, J. K., Reynald, R. L., Schoch, G. A., Griffin, K. J., Stout, C. D., and Johnson, E. F. (2007) *J. Biol. Chem.* **282,** 14348–14355
11. Wester, M. R., Johnson, E. F., Marques-Soares, C., Dijols, S., Dansette, P. M., Mansuy, D., and Stout, C. D. (2003) *Biochemistry* **42,** 9335–9345
12. Collaborative Computational Project, Number 4 (1994) *Acta Crystallogr. D Biol. Crystallogr.* **50,** 760–763
13. McCoy, A. J., Grosse-Kunstleve, R. W., Storoni, L. C., and Read, R. J. (2005) *Acta Crystallogr. D Biol. Crystallogr.* **61,** 458–464
14. Sali, A., Potterton, L., Yuan, F., van Vlijmen, H., and Karplus, M. (1995) *Proteins* **23,** 318–326
15. Brünger, A. T., Adams, P. D., Clore, G. M., DeLano, W. L., Gros, P., Grosse-Kunstleve, R. W., Jiang, J. S., Kuszewski, J., Nilges, M., Pannu, N. S., Read, R. J., Rice, L. M., Simonson, T., and Warren, G. L. (1998) *Acta Crystallogr. D Biol Crystallogr.* **54,** 905–921
16. Cosme, J., and Johnson, E. F. (2000) *J. Biol. Chem.* **275,** 2545–2553
17. von Wachenfeldt, C., Richardson, T. H., Cosme, J., and Johnson, E. F. (1997) *Arch. Biochem. Biophys.* **339,** 107–114
18. Williams, P. A., Cosme, J., Sridhar, V., Johnson, E. F., and McRee, D. E. (2000) *Mol. Cell* **5,** 121–131
19. Thomas, J. H. (2007) *PLoS Genet.* **3,** e67
20. Goldstone, H. M., and Stegeman, J. J. (2006) *J. Mol. Evol.* **62,** 708–717
21. Wang, R., Lai, L., and Wang, S. (2002) *J. Comput. Aided Mol. Des* **16,** 11–26
22. Bauer, E., Guo, Z., Ueng, Y. F., Bell, L. C., Zeldin, D., and Guengerich, F. P. (1995) *Chem. Res. Toxicol.* **8,** 136–142
23. Andries, M. J., Lucier, G. W., Goldstein, J., and Thompson, C. L. (1990) *Mol. Pharmacol.* **37,** 990–995
24. Kleywegt, G. J., and Jones, T. A. (1994) *Acta Crystallogr. D Biol. Crystallogr.* **50,** 178–185
25. Porubsky, P. R., Meneely, K. M., and Scott, E. E. (2008) *J. Biol. Chem.* **283,** 33698–33707
26. Schoch, G. A., Yano, J. K., Wester, M. R., Griffin, K. J., Stout, C. D., and Johnson, E. F. (2004) *J. Biol. Chem.* **279,** 9497–9503
27. Tu, Y., Deshmukh, R., Sivaneri, M., and Szklarz, G. D. (2008) *Drug Metab. Dispos.* **36,** 2371–2380
28. Petrek, M., Kosinová, P., Koca, J., and Otyepka, M. (2007) *Structure* **15,** 1357–1363
29. Wester, M. R., Johnson, E. F., Marques-Soares, C., Dansette, P. M., Mansuy, D., and Stout, C. D. (2003) *Biochemistry* **42,** 6370–6379
30. Luch, A., Coffing, S. L., Tang, Y. M., Schneider, A., Soballa, V., Greim, H., Jefcoate, C. R., Seidel, A., Greenlee, W. F., Baird, W. M., and Doehmer, J. (1998) *Chem. Res. Toxicol.* **11,** 686–695
31. Lee, A. J., Cai, M. X., Thomas, P. E., Conney, A. H., and Zhu, B. T. (2003) *Endocrinology* **144,** 3382–3398